Evaluating Yangtze River Delta Urban Agglomeration flood risk using hybrid method of AutoML and AHP

Yu Gao [1,2], Haipeng Lu [1,2], Yaru Zhang[1,2], Hengxu Jin[1,2], Shuai Wu[3], Yixuan Gao[1,2], Shuliang Zhang[1,2*]

1 Key Laboratory of VGE of Ministry of Education, Nanjing Normal University, Nanjing 210023, China

2 Jiangsu Center for Collaborative Innovation in Geographical Information Resource Development and Application, Nanjing 210023, China

3 Lianyungang Real Estate Registry, Lianyungang 222006, China

Correspondence to: Shuliang Zhang (zhangshuliang@njnu.edu.cn)

Abstract. With rapid urbanization, the scientific assessment of disaster risk caused by flooding events has become an essential task for disaster prevention and mitigation. However, adaptively selecting optimal machine learning (ML) models for flood risk assessment and further conducting spatial and temporal analyses of flood risk characteristics in urban agglomerations remain challenging. This study, establishes a "H–E–V–R" risk assessment index system that integrates hazard, exposure, vulnerability, and resilience based on the factors influencing flood risk in the Yangtze River Delta Urban Agglomeration (YRDUA). Utilizing Automated Machine Learning (AutoML) and the Analytic Hierarchy Process (AHP), a comprehensive flood risk assessment model is constructed. Results indicate that, among those of different assessment models, the accuracy, precision, F1-score, and kappa coefficient of the Categorical Boosting (CatBoost) model for flooded point identification are the highest. Among the flood hazard factors, elevation ranks highest in importance, with a contribution rate of up to 68.55%. The spatial distribution of flood risk in the study area from 1990 to 2020 is heterogeneous, with an overall increasing risk trend. This study is of great significance for advancing disaster prevention, mitigation, and sustainable development in the YRDUA.

1 Introduction

Under global climate change and accelerated urbanization, China has been experiencing pervasive flooding ever more frequently (Tang et al., 2024). Floods threaten people's lives, hinder social development and cause huge economic losses in China (Anon, 2021; Echendu, 2020; Milanesi et al., 2015). Flood formation has been exacerbated by climate change and urbanization, leading to increased frequency, extent, and intensity of urban flooding, and impacting urban flood risk (Mahmoud and Gan, 2018; Khadka et al., 2023; Scott et al., 2023; Seemuangngam and Lin, 2024). Modern human society is faced with the possibility of serious flood hazards and associated challenges, and in addition to post-disaster emergency management, the scientific assessment of disaster risks arising from flood events has gradually become a crucial aspect in preventing and mitigating disasters.

34   Currently, most research in the field of flooding focuses on the flood risks of individual cities (Wang et

35   al., 2021, 2023b; Guan et al., 2024). However, in recent years, the frequency and intensity of urban

36   flooding in China have increased dramatically, and individual cities are no longer able to independently

37   mitigate the risks arising from floods. Studies indicate that China's flood risk management needs to be

38   transformed from the scale of isolated individual cities to the scale of urban agglomerations, conducted

39   in a regionally coordinated manner (Morales-Torres et al., 2016; Wang et al., 2023a). City clusters,

40   constituting the spatial organizational structure of cities that have reached an advanced stage of

41   development, have become key areas for regional disaster management and sustainable development.

42   Due to the unique geographical location and climate conditions of the YRDUA, as well as the impact of

43   urbanization over the past 30 years, the frequency and intensity of flood disasters have been increasing,

44   posing a serious threat to the sustainable development of cities. Therefore, implementing relevant

45   emergency management strategies for flood risks is urgently needed. Furthermore, the region comprises

46   multiple cities, among which distinct resource interactions, such as population mobility and risk transfer,

47   exist (Lu et al., 2022). Thus, it is essential to assess both the overall flood risk characteristics and changes

48   in the urban agglomeration, as well as the spatial correlations of flood risks between cities, explore the

49   mutual influences and interaction mechanisms among regional disaster risks, and provide a scientific

50   basis for sustainable development within the urban agglomeration (Xu et al., 2024).

51   Statistical analyses of historical disaster statistics (Lang et al., 2004), indicator systems methods (Wang

52   et al., 2018), scenario simulations methods (Yang et al., 2018), and data-driven methods (Abu-Salih et

53   al., 2023), are the primary flood risk assessment method currently. With the development of artificial

54   intelligence technology, data-driven methods, such as machine learning, deep learning, and artificial

55   neural networks, have emerged, providing new opportunities for improving traditional flood risk

56   assessment methods (Liu Jiafu and Zhang Bai, 2015). Through continuous improvement and

57   development of machine learning algorithms, ensemble methods have effectively addressed the

58   limitations of traditional machine learning models (Kazienko et al., 2015). Various integrated ML

59   methods have been utilized in hydrology, with the Boost algorithm being extensively applied for flood

60   prediction and assessment (Shafizadeh-Moghadam et al., 2018; Mirzaei et al., 2021; Yan et al., 2024).

61   However, these integrated models lack preprocessing and feature selection capabilities, and their

62   application effects vary considerably across different regions. To fully mine data and discover more

63 effective features, experts have proposed other solutions, namely hybrid models such as ANFIS, LSTM-

64 ALO, and LSSVM-GSA (Nayak et al., 2004; Yuan et al., 2018; Adnan et al., 2017). These methods have

65 achieved good performances for given hydrological time series, focusing more on data preprocessing and

66 feature selection. Although research on data-driven urban flood risk assessment methods has increased,

67 certain limitations remain. For example, the physical importance of urban hydrological processes is often

68 ignored in the model assessment process, interpretation of the assessment results is weak, and quantifying

69 the boundaries and scales is challenging (Abu-Salih et al., 2023; Guo et al., 2022).

70 Furthermore, attempting to combine the data processing and feature selection capabilities of hybrid

71 models with those of integrated models remains challenging (Li et al., 2017). Existing algorithms cannot

72 perform well for all learning problems; thus, each ML component, such as feature engineering, model

73 selection, and algorithm selection, must be carefully configured (Li et al., 2017; Raschka, 2020). Hence,

74 ML applications require the participation of many experts, leading to disproportionate costs for ML

75 development and improvement (Wagenaar et al., 2020; Sarro et al., 2022; Rashidi Shikhteymour et al.,

76 2023). The effectiveness of machine learning "automatically improves with experience," and a key

77 challenge in the research is how to integrate the data processing capabilities and feature selection

78 strengths of hybrid models with ensemble models (Jordan and Mitchell, 2015; Nagarajah and Poravi,

79 2019). AutoML is an innovative ML framework designed for training ML models and addressing various

80 problems (He et al., 2021; Consuegra-Ayala et al., 2022). However, AutoML has not been widely applied

81 in the fields of hydrology and disaster risk management, and research has mainly focused on optimizing

82 the integrated model to achieve better performance (Özdemir et al., 2023). Continuous research has

83 highlighted the potential role of AutoML in flood risk detection and assessment (Guo et al., 2022; Vincent

84 et al., 2023; Munim et al., 2024). Guo et al. (2022) compared AutoML with three single ML algorithms

85 (CatBoost, XGBoost, and BPDNN) and concluded that AutoML performed better in building rapid

86 warning and comprehensive analysis models for urban waterlogging. The model based on AutoML can

87 be applied to areas without water level monitoring and achieve accurate predictions and rapid warnings

88 of waterlogging depth (Guo et al., 2022; Yan et al., 2024). Abu-Salih et al. (2023) proposed a data-driven

89 flood risk area detection model that combined the integrated model with the AutoML tool and

90 successfully solved the problems of data balance and strategy modeling, while reducing the complexity

91 of flood risk area prediction.   Previous studies have provided a theoretical basis and scientific reference

92   for the application of AutoML methods to flood risk assessment. However, the use of AutoML for

93   research purposes is a complex issue, and many new opportunities and challenges remain regarding its

94   specific applications.

95   Although AutoML can objectively and efficiently calculate flood risk, it lacks comprehensiveness and

96   judgment. Therefore, when evaluating the indicators of various dimensions of flood risk, quantifying the

97   impacts of different levels of each indicator on flood risk is impossible, and determining the indicator

98   weight is challenging. Therefore, to determine the indicator weight, using relevant statistical methods is

99   necessary. Multicriteria decision analysis (MCDA) is a useful tool for considering complex decision-

100   making problems in flood risk management (Fernández and Lutz, 2010). The analytic hierarchy process

101   (AHP) is one of the most popular MCDA techniques (Donegan et al., 1992). This technique emphasizes

102   the importance of the subjective judgment of decision makers and the consistency of pairwise

103   comparisons of standards in the decision-making process (Saaty, 1980). Recent studies have focused on

104   integrated frameworks of ML models and MCDA technology for flood hazard assessment (Kanani-Sadat

105   et al., 2019; Khosravi et al., 2019; Gudiyangada Nachappa et al., 2020; Mia et al., 2023). However,

106   research focusing on using an integrated framework of AutoML and AHP techniques is still limited.

107   This study constructs a flood risk assessment model based on AutoML and AHP by examining the factors

108   influencing flood risk in the YRDUA. Based on the proposed flood risk assessment model, the risk,

109   exposure, vulnerability, and resilience as well as their corresponding weights of flooding in the YRDUA

110   are calculated, and the regional flood risk level zoning map is obtained. The comparative analysis of

111   superimposed flooded points data shows a strong alignment between the distribution of flooded points

112   in the study area and the high to medium-high risk areas, highlighting the reliability and applicability of

113   the proposed model. The remainder of this paper is structured as follows: Section 2 describes the study

114   area, data sources, and methodology; Section 3 presents the results and analysis; Section 4 discusses the

115   findings and their implications; and Section 5 concludes the study with key insights and

116   recommendations.

117   **2 Materials and methods**

118   In this section, the study area is briefly introduced (Section 2.1), and each individual component of the

119   study is further discussed along with the basic geographic information, meteorology, social statistics,

120 historical disaster data, and other fields involved in the study of urban agglomeration flood disasters and

121 their risks (Section 2.2). The framework of the flood risk assessment model is shown in **Figure 1**. The

122 factors influencing flood risk in the YRDUA are explored, and a flood risk assessment index system is

123 established (Section 2.3). The optimal model in AutoML is selected to calculate the importance of flood

124 hazard and hazard characteristic factors (Section 2.4), and the model is combined with AHP to determine

125 the weight of each risk indicator (Section 2.5). Ultimately, a flood risk assessment model based on

126 AutoML and AHP is constructed.

127
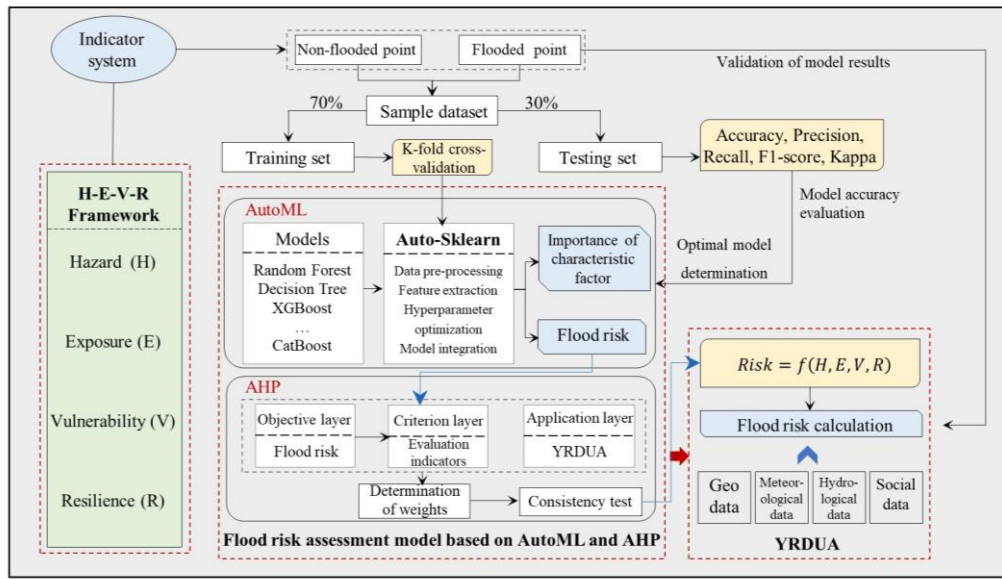
128 **Figure 1: Flood risk assessment modeling framework.**

129

130 **2.1 Study area**

131 The Yangtze River Delta Urban Agglomeration, located in the eastern coastal region of China (27° 04′–

132 34° 49′ N; 115° 75′–122° 95′ E), includes 27 cities: 8 in Anhui Province, 9 in Jiangsu Province, 9 in

133 Zhejiang Province, and Shanghai (**Figure 2**) (Yang et al., 2024). Influenced by the East Asian summer

134 monsoon, the study area features low-lying plains in the northern region and higher hilly terrain in the

135 southern region, along with numerous waterways (Ding et al., 2021). With the recent accelerated climate

136 change and urbanization, extreme precipitation events in the Yangtze River Delta (YRD) have been

137 occurring ever more frequently, and the temporal and spatial distribution differences in precipitation have

138 increased. Additionally, the increase in impervious surfaces, narrow plains rivers, and poor drainage may

139 result in more frequent and widespread urban flooding and waterlogging disasters (Wan et al., 2013).

140 This region is economically developed and densely populated , making it the largest urban agglomeration

141 in Asia (Sun et al., 2023). In 2008, the Gross Domestic Product (GDP) of the YRD accounted for 17.5%

142 of the GDP of the entire country, i.e., 4.3 trillion yuan, and the per capita GDP was 44,468 yuan, i.e.,

143 twice the national average level. The population has reached 97.2 million, i.e., 7.3% of China's total

144 population, and the region's average population density is 877 persons/km^2, i.e., approximately twice the

145 national average (Gu et al., 2011). Therefore, the potential risks of flood and waterlogging disasters are

146 substantial.

147
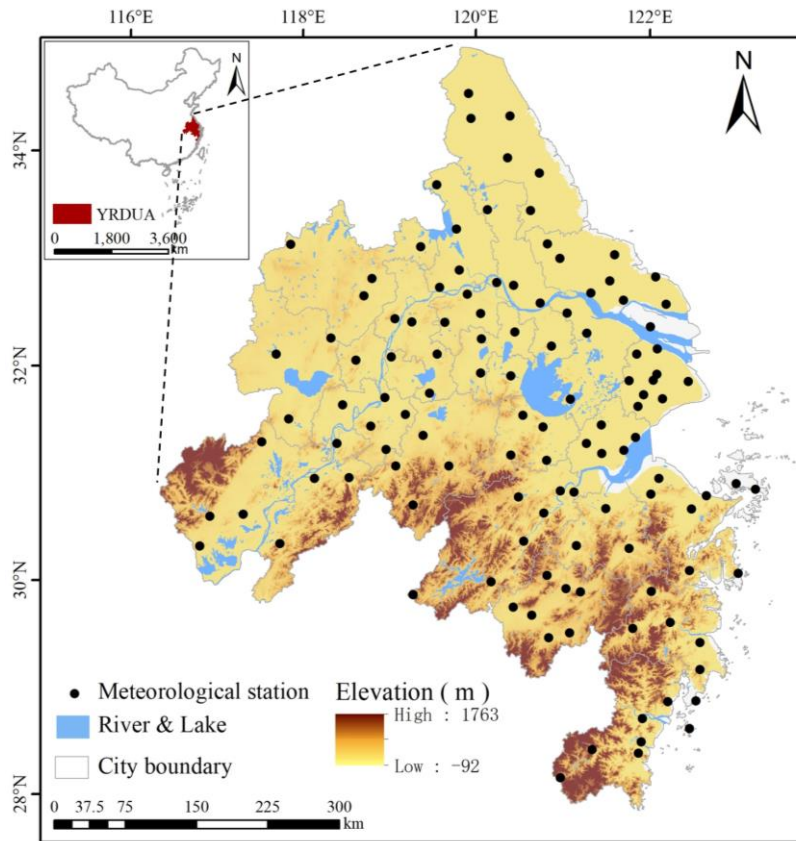
148 **Figure 2: The schematic map of the YRDUA.**

149

150 **2.2 Data sources and processing**

151 **2.2.1 Data sources**

152 The study of flood disasters and their associated risks in urban agglomerations involves complex natural

153 and socio-economic factors. Therefore, we collected and preprocessed data from multiple fields, such as

154 basic geography, meteorology, social statistics, and historical disasters. **Table 1** lists the data types and

155 resolutions collected for the research area.

156 **Table 1: Description of the Datasets Used for Flood Risk Assessment, Their Characteristics, and Data Sources.**

Category	Details	Resolution	Data Source
Basic Geographic Information Data	Administrative boundaries and river network density data.	30m	-Resources and Environmental Science and Data Center, CAS (https://www.resdc.cn/). -USGS (https://earthexplorer.usgs.gov/). -Wuhan University CLCD dataset (https://zenodo.org/records/8176941). - National Ecosystem Science Data Center (nesdc.org.cn).
	Digital Elevation Model (DEM) based on SRTM1 (30m), mosaicked and clipped to the study area (27 core cities).		
	Land use data from CLCD (30m), includes 7 types: farmland, forest, shrubland, grassland, water, bare land, and impervious surfaces.		
	NDVI data (2000–2020) calculated using the GEE platform.		
Meteorological Data	Hourly precipitation data from 120 meteorological stations. Data preprocessed for outlier removal and missing value handling.	Station data	National Meteorological Information Center, China Meteorological Administration
Social Statistics	Population, unemployment, GDP, and healthcare statistics at the prefecture level.	Prefecture-level	Provincial and municipal statistical yearbooks and bulletins
	Urbanization rate calculated using urban population proportion.		
	GDP density and per capita GDP derived from total GDP and land area/population.		
Historical Disaster Data	Flood inundation data from the MODIS-based Global Flood Database (2000–2018), processed to focus on the YRDUA region. To ensure comprehensive selection of inundation points, the inundated areas within the time frame were overlaid to produce a historical flood map.	250m	Global Flood Database (https://www.emdat.be/).

157

158 **2.2.2 Data standardization and preprocessing**

159 Due to variations in data sources and formats, the collected flood disaster risk data exhibit differences in

160 spatial resolution, dimensions, and magnitude. To ensure consistency and comparability, standardization

161 of both spatial scale and numerical range was performed before using these datasets as flood risk

162 indicators.

163 Unification of spatial scale means aligning data within the same coordinate range and resolution. The

164 research data is standardized through projection transformation, converting all datasets into the same

165 geographic and projected coordinate systems. The Kriging interpolation method is used to spatially

166 process all discrete data. Finally, if the spatial data has different resolutions, resampling is performed to

167 standardize all data to the same resolution, which in this study is unified to 30m×30m.

168 Normalization of the numerical range can be achieved using a normalization process. Through a linear

169 transformation, the values of the data are mapped to the range [0, 1], thus eliminating the influence of

170 differing dimensions among the data indicators. In this study, the Min-Max Normalization method is

171 used for normalization, and the formula is given by Eq. (1) :

$$x' = \frac{x - \min(x)}{\max(x) - \min(x)}, \tag{1}$$

172 **2.3 Extraction of historical flood inundation points**

173 The historical flood inundation map of the study area is shown in **Figure 3** (a). The flood inventory map

174 used in this study was created based on inundation data from the Global Flood Database and the EM-

175 DAT flood disaster database, and further verified through satellite imagery, Google Earth, and existing

176 historical flood records. The actual flooded areas were delineated from flood traces in the inundation

177 dataset and image interpretation. During the study period, 278 flooded points were randomly selected

178 within the inundation data range. The location of each point serves as the foundation for subsequent

179 statistical analysis of flood events, with the spatial distribution shown in **Figure 3** (b).

180 To calculate flood hazard, it is necessary to select training samples. The task of identifying flooded and

181 non-flooded points using AutoML is essentially a binary classification problem, which requires a

182 balanced number of samples. An imbalanced ratio of positive and negative samples can result in

183 unreliable classification outcomes. Previous studies (Pham et al., 2021; Bostan et al., 2012) have shown

184 that the best classification performance is achieved when the ratio of flooded to non-flooded points is

185 1:1. Therefore, after selecting the flooded points, 278 non-flooded points were randomly sampled to

186 ensure a balanced 1:1 ratio, excluding high-altitude areas, based on the region's actual characteristics.

187 Finally, the flooded and non-flooded points were used as sample data and divided into a 7:3 ratio (70%

188 for training and 30% for testing) for model training.
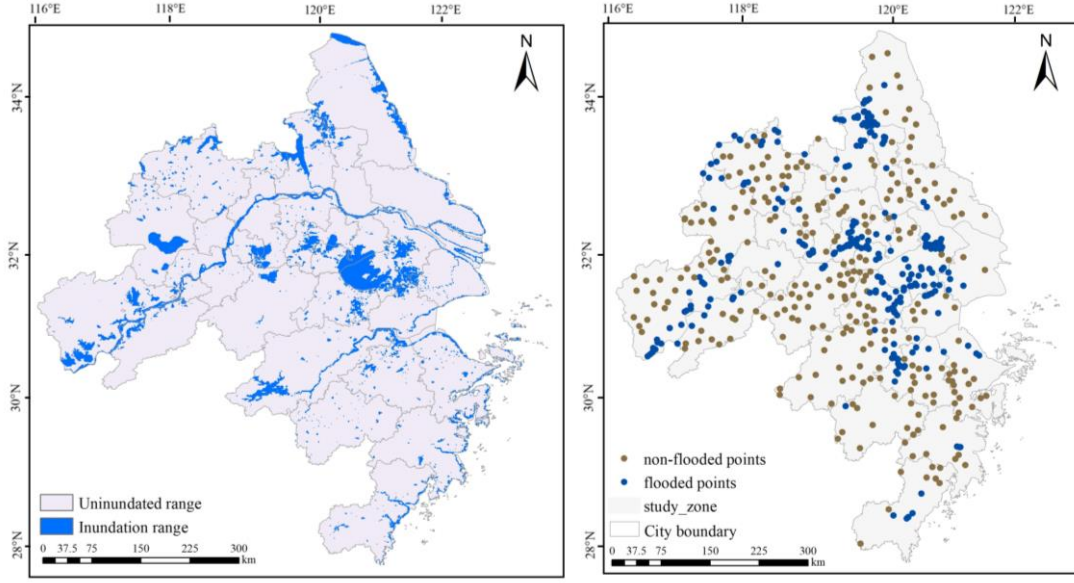
Figure 3: (a) Flood inundation map of the study area. (b) Spatial Distribution of Flooded and Non-Flooded Points in the YRDUA.

2.4 Establishment of a flood risk assessment indicator system

Although risk is a universal concept, it has no universal definition (Aven, 2016; Mishra and Sinha, 2020). Based on the hazard–exposure–vulnerability (H–E–V) disaster risk framework, we considered the particularity of flood risk research at the urban agglomeration scale, incorporated resilience indicators into the existing framework, and constructed a four-dimensional flood risk assessment framework of hazard–exposure–vulnerability–resilience (H–E–V–R) that can assess regional flood risks more comprehensively and systematically. The conceptual description of flood risk in this study can be expressed in the Eq. (2):

$$Risk = f(H, E, V, R) = \sum_{i=1}^{a} \omega_H H_i + \sum_{i=1}^{b} \omega_E E_i + \sum_{i=1}^{c} \omega_V V_i + \sum_{i=1}^{d} \omega_R R_i, \tag{2}$$

where H, E, V, and R represent the danger of, exposure to, vulnerability to, and resilience in response to floods, respectively; ω_H, ω_E, ω_V, and ω_R are the weights of danger, exposure, vulnerability, and resilience, respectively; H_i, E_i, V_i, and R_i are the values of items i of the indicators, respectively; and a, b, c, and d are the numbers of the indicators, respectively.

We constructed a flood risk assessment index system for the YRDUA based on the "H–E–V–R" framework, the actual situation of the study area, the formation mechanisms of flood disasters, and the findings of relevant studies (Gain et al., 2015; Criado et al., 2019; Hsiao et al., 2021). We selected four

first-level indicators (i.e., hazard, exposure, vulnerability, and resilience indices) and 19 second-level

indicators. A detailed description of the flood risk assessment index system is presented in **Figure 4**.
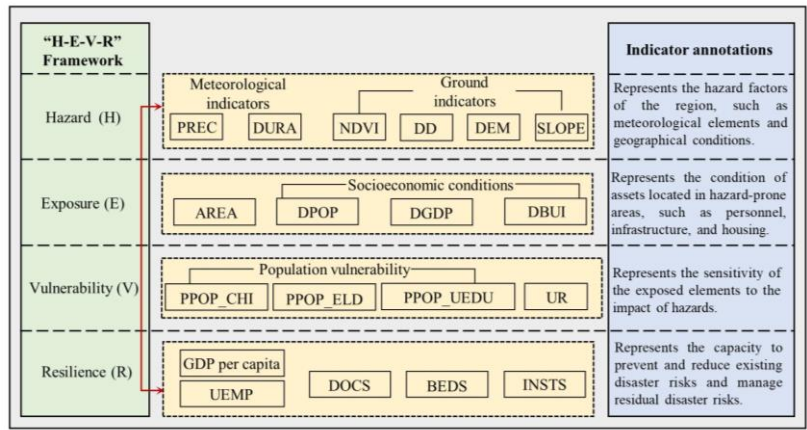
Figure 4: Flood risk assessment index system for the YRDUA based on the H–E–V–R framework.

The hazard indicators consisted of six indices: Average annual precipitation (PREC), Annual Cumulative

Heavy Rainfall Duration (DURA), Digital Elevation Model (DEM), SLOPE, Drainage Density (DD),

and Normalized Difference Vegetation Index (NDVI). Rainfall is the primary factor leading to flooding,

particularly extreme rainstorms caused by climate change. According to the Meteorological Bureau's

definition, a heavy rainstorm event is characterized by rainfall of 50mm or more within 24 hours. DURA

is defined as the total number of days with heavy rainstorm events occurring at all meteorological stations

within the study area each year. The more days heavy rainstorms accumulate and the longer their

duration, the greater the likelihood of flooding and other disaster events. DEM and SLOPE are important

topographical indicators. Areas with low DEM and SLOPE values are generally more susceptible to

flood threats. DD refers to the area of rivers or lakes per unit of land surface area and is a crucial indicator

of a watershed's structural characteristics. It determines the watershed's capacity to withstand flooding.

The higher the DD, the greater the likelihood of flooding and the higher the potential flood risk.

Vegetation plays a role in water storage, retention, and infiltration. The lower the vegetation coverage,

the weaker the buffering capacity, making it more likely for surface water to accumulate. The NDVI

index measures the relative abundance of green vegetation, with values ranging from -1 to 1. The higher

the value, the greater the vegetation coverage, and the lower the risk of flooding.

Land area (AREA), Population Density (DPOP), GDP Density (DGDP), and Building Density (DBUI)

were selected as exposure indicators to assess the degree of vulnerability of both the natural environment

231 and social systems to flooding. The land area for each administrative unit at the prefecture-level city is

232 calculated individually. A larger land area corresponds to a greater extent exposed to flooding. DPOP

233 and DGDP represent the concentration of population and assets, respectively. Areas with higher DPOP

234 and DGDP are more susceptible to potential threats from pluvial flooding. DBUI, the ratio of total

235 building area to total land area in a region, indicates the building density. A higher DBUI reflects greater

236 exposure to flooding.

237 Vulnerability indicators focus more on the social aspects of flood disasters. This study selects four

238 vulnerability indicators: Proportion of Child Population (PPOP_CHI), Proportion of Elderly Population

239 (PPOP_ELD), Proportion of Uneducated Population (PPOP_UEDU), and Urbanization Rate (UR). Age

240 is a key feature of social vulnerability, and both the population aged 0-14 and those over 65 are considered

241 vulnerable groups, as these age groups are more susceptible to flood damage. The uneducated population

242 generally has a weaker awareness of disaster risks and lower self-protection capacity, which makes this

243 group more vulnerable to flooding. The urbanization rate refers to the proportion of the urban population

244 in the total resident population of a region. This indicator is inversely related to flood vulnerability. In

245 general, a higher urbanization rate indicates greater social development and stronger protective

246 capacities, which can reduce vulnerability to flooding to some extent.

247 The resilience indicators selected in this study include Gross Domestic Product (GDP) per capita,

248 Unemployment Rate (UEMP), Number of Doctors (DOCS), Number of Medical Institutions (INSTS),

249 and Number of Hospital Beds (BEDS). GDP per capita is the ratio of a region's GDP to its total resident

250 population over a specified period, reflecting the region's economic condition. A higher GDP per capita

251 indicates a more developed economy, which is associated with a greater capacity to recover quickly after

252 a flooding event. The Unemployment Rate (UEMP) measures the proportion of the idle labor force,

253 indirectly reflecting the stability of urban development. A high unemployment rate signals economic

254 instability, which weakens the capacity to cope with floods and extends the time required for post-disaster

255 recovery, thus impeding disaster response efforts. The indicators of DOCS, INSTS, and BEDS provide

256 insights into a region's healthcare and medical support capabilities. Areas with stronger healthcare

257 systems are better positioned to manage flood risks and recover more effectively from such disasters.

258

259 **2.5 Flood risk calculation method based on AutoML**

260 **2.5.1 Feature selection**

261 The flood inventory map in this paper was developed using inundation data from the Global Flood

262 Database and flood disaster data from the EM-DAT database, supplemented by satellite and Google

263 image interpretation and verified against existing historical flood records. The actual flood-affected areas

264 were delineated based on flood traces from the inundation datasets and image interpretations. For this

265 study, 278 flood inundation points were randomly selected within the inundation data range during the

266 study period, and the location of each point was used as the basis for subsequent statistical analysis of

267 flood events. The main factors affecting flood risk were considered during input feature selection.

268 Rainfall and rainstorms are important factors that lead to floods, and flooding is closely related to

269 topography, slope, vegetation cover, and hydrological conditions. Therefore, six indicator factors,

270 namely PREC, DURA, DEM, SLOPE, NDVI, and DD, were selected as the input features of the model.

271 To verify the model, 70% of the data in the sample were set as the training dataset and the remaining

272 30% of the data were set as the testing dataset through random sampling.

273 When the number of samples is small, data balancing is essential to ensure uniform sampling and reduce

274 the deviations among the training, validation, and original datasets. Data balancing refers to the process

275 of achieving a balanced distribution of data for each labeled category; it is particularly important when

276 the number of observations in each class is significantly different. One way to address an imbalanced

277 dataset is to oversample the minority classes. In this study, we assessed flood risk based on the

278 identification of flooded point in the sample, which is essentially a binary classification problem;

279 therefore, the output features are 0, i.e., negative categories (non-flooded points), versus 1, i.e., positive

280 categories (flooded points). The processed dataset comprised 278 positive samples (flooded points) and

281 278 negative samples (non-flooded points), with each label consisting of 278 points representing the

282 entire dataset.

283 **2.5.2 Model training and hyperparameter optimization**

284 Training samples were generated using the data from flooded and non-flooded points in the study area,

285 and the Auto-Sklearn was used for model training, its principle is shown in **Figure 5**. The Auto-sklearn

286 framework has multiple built-in machine learning algorithms. We selected 9 models that are more typical

287 or have better performance in flood hazard research: random forest (RF), extreme gradient boosting

288 (XGBoost), Light Gradient Boosting Machine (LightGBM), categorical feature boosting (CatBoost),

289 Extra trees, Decision tree, Nearest Neighbors, Multi-layer Perceptron (MLP) neural network, and Linear

290 Regression. The training and testing datasets were used to train the 9 machine learning models, and the

291 hyperparameters were continuously adjusted and optimized.

292
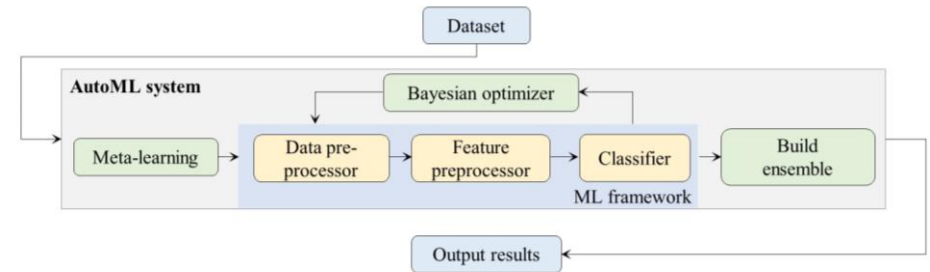
293 **Figure 5: Principles of Auto-Sklearn**

294

295 Hyperparameter optimization is an important step in ML model training. The aim of this step is to

296 determine a hyperparameter combination to generate a ML model that performs well on a specific dataset

297 and reduces the effect of the predefined loss function on a given dataset. In this study, we used a grid

298 search strategy for optimization. For each set of hyperparameter combinations, k-fold cross-validation

299 was used to evaluate the model and determine the hyperparameter combination of the optimal model that

300 achieved the best balance of Precision, Recall, and F1-score. Briefly, the training dataset was divided

301 into K parts, of which one was selected as the test set and the rest were used as the training set. The cross-

302 validation was repeated K times and the results were averaged K times. The model with the best average

303 result among all models was selected as the optimal model, and the final classification prediction result

304 was the output. In this study, we used 5-fold cross-validation.

305 **2.5.3 Performance evaluation**

306 To better compare the performance of the 9 selected ML models in the Auto-Sklearn framework for flood

307 risk assessment, multiple evaluation indicators were used to assess the test dataset. The following

308 combinations of the true category of the sample point and the category predicted by the classifier were

309 used: True Positive (TP)—the sample point is a flooded point, and the model classifier also predicts that

310 it is a flooded point; True Negative (TN)—the sample point is a non-flooded point, and the model

311 classifier also predicts that it is a non-flooded point; False Positive (FP)—the sample point is a non-

312 flooded point, and the model classifier mistakenly predicts that it is a flooded point; False Negative

313 (FN)—the sample point is a flooded point, and the model classifier mistakenly predicts that it is a non-

314 flooded point. Therefore, four related indicators were selected: Precision, Recall and F1-score, and the

315 consistency metric Kappa coefficient. The calculation formulas are given in Eq. (3), Eq. (4), and Eq. (5):

$$Precision = \frac{TP}{TP+FP} \ , \tag{3}$$

$$Recall = \frac{TP}{TP+FN} \ , \tag{4}$$

$$F1-_{score} = \frac{2TP}{2TP+FP+FN} \ , \tag{5}$$

316 Among the indicators, *Precision* refers to the proportion of correctly predicted flooded points among all

317 predicted flooded points, reflecting the model's ability to avoid false positives. *Recall* measures the

318 proportion of correctly identified flooded points among all actual flooded points, representing the

319 model's sensitivity. *F1-score* is the harmonic mean of Precision and Recall, providing a balanced

320 evaluation of both metrics and reflecting the overall recognition performance of the model.

321 *Kappa* coefficient is a statistical consistency metric used to measure classification performance, which

322 is calculated based on the confusion matrix of true and predicted categories. Its value ranges from [-1,1]:

323 A Kappa value of 1 indicates perfect agreement, 0 means the classification is no better than random

324 guessing, and negative values suggest the classification is worse than random prediction. *Kappa* is

325 calculated using Eq. (6), where P_e is given by Eq. (7).

326 $$Kappa = \frac{P_o - P_e}{1 - P_e}, \tag{6}$$

327 $$P_e = \frac{(TP+FP)(TP+FN)+(TN+FN)(TN+FP)}{(TP+FP+TN+FN)^2}, \tag{7}$$

328 where P_e represents the expected agreement by chance.

329 Combining multiple indicators allows for a more comprehensive evaluation of models within the Auto-

330 Sklearn framework for flood point identification and flood risk assessment.

331 **2.6 Method for determining flood risk index weights based on AHP**

332 **2.6.1 Establishing a hierarchical model**

333 According to the decision-making objectives, factors, and applications in decision-making problems, the

334 AHP can be divided from bottom to top into the target, criterion, and application layers. Among them,

335   the target layer is the problem to be solved (i.e., final flood risk). The criterion layer is the intermediate

336   link, including the factors to be considered and the decision making criteria. The factors can be divided

337   into different evaluation indicators, including four first-level indicators (danger, exposure, vulnerability,

338   and resilience) and their corresponding 19 second-level indicators. The criterion layer comprises various

339   weight combination schemes linked to the target layer. The application layer is the final optional scheme

340   and specific application of the decision. The final weight scheme and evaluation results of this study

341   were applied to the YRDUA.

342   **2.6.2 Constructing the judgment matrix**

343   After the hierarchical structure was established, a judgment matrix was constructed based on the

344   relationship between the criteria and indicators. Different elements in the sublevel were compared

345   pairwise, and the relative importances of all elements in the current layer and previous layer were

346   compared. Typically, a pairwise comparison matrix is used as representative. In this study, we adopted

347   the 1–9 scale method as the importance measurement standard. The importance comparison relationship

348   is presented in **Table 2**, where the matrix element a_{ij} represents the comparison result of the ith element

349   relative to the jth element.

350   **Table 2: Pairwise comparison point-based rating scale of AHP.**

Ranking	Importance Level
1	Equally important
3	i is slightly more important than j
5	i is much more important than j
7	i is very much more important than j
9	i is extremely important than j
2, 4, 6, 8	Intermediate value of two adjacent judgments
Reciprocal	Comparative judgment of j vs., $a_{ji} = 1/a_{ij}$

351

352   **2.6.3 Solving the eigenvector of the judgment matrix**

353   Based on the judgment matrix, the square root method was used to solve the eigenvector and eigenvalue.

354   The first step is to calculate the square root a_{ij} of the product of each row of the judgment matrix n,

355 then normalize it, and finally calculate the maximum eigenvalue of the judgment matrix. The formula is

356 as Eq. (8), Eq. (9), Eq. (10).

357 $$M_i = \sqrt[n]{\prod_{j=1}^{n} a_{ij}}, \tag{8}$$

358 $$W_i = \frac{M_i}{\sum_{i=1}^{n} M_i}, \tag{9}$$

359 $$\lambda_{max} = \sum_{i=1}^{n} \frac{(AW)_i}{nW_i}, \tag{10}$$

360 **2.6.4 Consistency check**

361 After the eigenvector calculation is completed, a consistency test is required to reduce the subjectivity in

362 the judgment matrix and enhance the scientific nature of the data and calculations. In a pairwise

363 comparison matrix, consistency means that the decision-maker's judgments must exhibit logical

364 coherence and transitivity. Specifically, if option A is considered more important than option B, and

365 option B is considered more important than option C, then consistency requires that option A must also

366 be judged more important than option C (Saaty, 1984).

367 The consistency indicator (CI) is used to measure the deviation of the judgment matrix from the

368 consistency: the smaller the CI, the greater the consistency of the judgment matrix. When CI = 0, the

369 judgment matrix is completely consistent. The CI calculation formula is as Eq. (11).

370 $$CI = \frac{\lambda_{max} - n}{n-1}, \tag{11}$$

371 To quantify the standard, the relative consistency (CR) index was further calculated as Eq. (12).

372 $$CR = \frac{CI}{RI}, \tag{12}$$

373 Where average Random Consistency Index (RI) represents the average random consistency which

374 depends only on the order of the judgment matrix. The RI values for judgment matrices of order 1 to 10

375 are shown in **Table 3**.

376 **Table 3: Consistency index (RI) for a randomly generated matrix.**

n	1	2	3	4	5	6	7	8	9	10
RI	0.00	0.00	0.52	0.89	1.12	1.26	1.36	1.41	1.46	1.49

377

378 CR was determined based on the RI value. When CR < 0.1, the consistency of the judgment matrix is

379 considered good. When CR > 0.1, the consistency of the judgment matrix is unacceptable, and the

380   judgment matrix must be adjusted and modified. In such cases, the corresponding judgment matrix was

381   further constructed, and the eigenvector and eigenvalue were calculated using the following formulas:

382   Finally, the judgment matrix that passed the consistency test was used to calculate the weights of the

383   indicators at the different levels.

384   **2.7 Determination of flood risk levels**

385   The classification of flood risk levels often involves manually setting thresholds, which can introduce

386   subjectivity and influence the accuracy of the risk assessment outcomes (Ma et al., 2022). To calculate

387   the flood risk, we employed the natural breakpoint classification method, which groups data into classes

388   based on natural divisions within the dataset (Lin et al., 2019). This method works by identifying points

389   where the data distribution changes most significantly and dividing the data into ranges based on these

390   breaks. Unlike clustering methods, which do not focus on the number and range of elements in each

391   group, the natural breakpoint method ensures that the range and number of elements in each group are as

392   balanced as possible (Ma et al., 2022).

393   **3 Results and discussion**

394   **3.1 Model flood risk results and evaluation**

395   **3.1.1 AutoML optimal model selection**

396   In the experiment, 9 typical ML models under the Auto-Sklearn framework were used to process the

397   sample dataset, with 70% of the sample set being used as the training dataset and 30% being used as the

398   testing dataset. The results of the comparative analysis of the model performance based on the test dataset

399   are presented in **Table 4**. A comprehensive analysis of the results on the testing data revealed that, in

400   terms of Precision, CatBoost had the highest value (0.9030), followed by LightGBM (0.8960) and Extra

401   Trees (0.8893). Meanwhile, CatBoost had the highest recall rate of 0.8883, followed by that of Extra

402   Trees at 0.8870. The probability thresholds for Precision, Recall, and F1-score range from [0,1], while

403   the Kappa coefficient ranges from [-1,1]. The F1-score and Kappa coefficient of the CatBoost model

404   were also markedly higher than those of the other models, reflecting the model's good consistency. A

405   comprehensive comparison showed that the precision, F1-score, and Kappa coefficient of the CatBoost

406   model were the highest, with its precision reaching 0.9030, indicating that the recognition and prediction

precision of the flooded points in the study area based on the CatBoost model were obviously better than those of other common machine learning models.

Since flood data often involve various environmental factors and complex interactions, the CatBoost model is highly effective at handling these intricate nonlinear relationships and feature interactions. Additionally, the model incorporates multiple regularization mechanisms during tree construction, which helps prevent overfitting and enhances the model's generalization capability. The results indicate that most models performed well on the training set, but their performance slightly declined on the test set, highlighting variations in generalization ability. CatBoost demonstrated strong robustness, achieving a Precision of 0.9319 on the training set and 0.9030 on the test set. Additionally, LightGBM and XGBoost showed relatively consistent performance between the training and test sets, suggesting better generalization. However, models such as Decision Tree and Nearest Neighbors exhibited a more significant performance drop in the test set, indicating a higher sensitivity to overfitting. To further evaluate overfitting, we used 5-fold cross-validation by comparing the performance of the training and testing sets. The experimental results indicate that while most models showed some performance decline on the test set, CatBoost maintained relatively stable performance, suggesting that the model does not exhibit significant overfitting and has good generalization ability.

Table 4: Comparative analysis of the performances of different ML models.

Models	Dataset	Precision	Recall	F1-score	Kappa
CatBoost	Training set	0.9319	0.9307	0.9547	0.8614
	Testing set	0.9030	0.8883	0.8960	0.7915
XGBoost	Training set	0.9017	0.8827	0.8818	0.8640
	Testing set	0.8748	0.8640	0.8624	0.7256
LightGBM	Training set	0.9349	0.9307	0.9306	0.8616
	Testing set	0.8960	0.7890	0.8015	0.7324
Random Forest	Training set	0.8922	0.8747	0.8745	0.7484
	Testing set	0.8482	0.8320	0.8309	0.6662
Extra Trees	Training set	0.8524	0.8240	0.8735	0.7695
	Testing set	0.8893	0.8870	0.8877	0.7751
Decision Tree	Training set	0.8886	0.8640	0.8621	0.8040
	Testing set	0.8810	0.8720	0.8708	0.7419

Models	Dataset	Precision	Recall	F1-score	Kappa
Linear Regression	Training set	0.8636	0.8533	0.8525	0.7073
	Testing set	0.8682	0.8480	0.8450	0.6926
Nearest Neighbors	Training set	0.7301	0.7907	0.7987	0.6009
	Testing set	0.7747	0.7440	0.7390	0.4937
MLP Neural Network	Training set	0.8998	0.8880	0.8873	0.7765
	Testing set	0.8682	0.8480	0.8450	0.6926

425

By comparing the performances of the 9 models, we found that the CatBoost model was more effective

in identifying flooded points. To further verify the excellent performance of the model, the receiver

operating characteristic (ROC) curve and area enclosed by the coordinate axes (corresponding area under

the curve [AUC] value) were plotted based on the test dataset to assess the model's binary classification

effectiveness: the larger the AUC value, the better the model distinguishes between classes. When AUC

> 0.8, the model prediction effect is very good (Sinha et al., 2008). In this study, both micro- and macro-

average ROC curves were plotted. The micro-average ROC curve aggregates the contributions of all

classes to compute the average ROC curve, treating each instance equally, while the macro-average ROC

curve computes the ROC curve for each class independently and then averages the results. These two

methods are commonly used for multi-class classification problems, but in this study, they were used to

give a more comprehensive comparison of model performance. The verification results are shown in

Figure 6. The AUC value of the CatBoost model reached 0.91, guaranteeing the performance and

prediction reliability of the CatBoost model. Based on this, the CatBoost model was selected to calculate

the flood risk in the YRDUA.
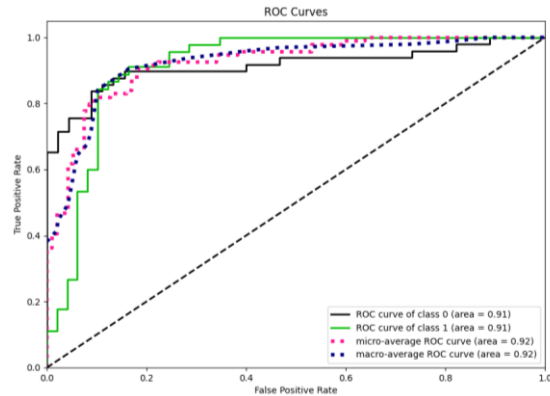
Figure 6: Receiver operating characteristic (ROC) curves and corresponding area under the curve (AUC)
values of the CatBoost model.

3.1.2 Importance and interpretability analysis of hazard factors

To better understand the contribution of different hazard indicators to flood risk in the YRDUA, we

conducted both importance ranking analysis using the CatBoost model and interpretability analysis based

on SHAP.

The CatBoost model was used to quantify the relative importance of six key hazard indicators. The results,

shown in **Figure 7**, reveal significant differences in their influence. DEM was identified as the most

critical factor, contributing 68.55%, which far exceeds the other factors, which is also in line with the

findings of many researchers within the region (Mei et al., 2021; Wan et al., 2013). Low-lying areas

naturally function as water accumulation zones, increasing flood vulnerability. Additionally, urban areas

in the YRDUA are dominated by impervious surfaces, limiting infiltration and exacerbating flood risks.

While PREC is a primary factor in storm-induced flooding, its direct contribution to flood risk was

relatively low compared to DURA, which accounted for 10.07%. This highlights that the persistence of

extreme rainfall events is a stronger predictor of flood hazard than total annual precipitation.
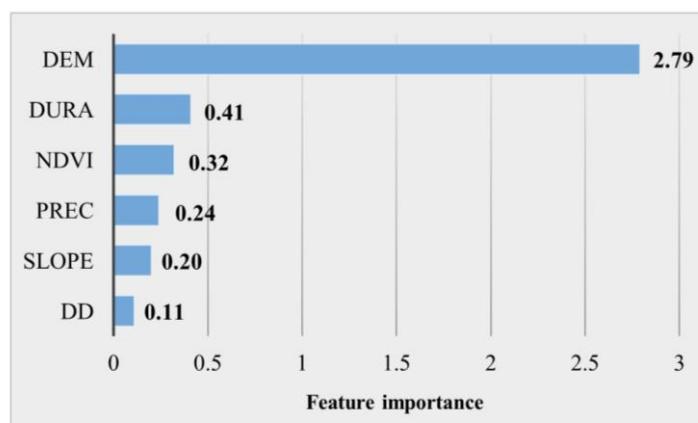
Figure 7: Importance Ranking of Hazard Factors Based on the CatBoost Model

To further analyze the interpretability of the model and understand the impact of individual flood hazard

indicators on the model's classification results, this paper calculates Shapley Additive Explanations

461 (SHAP) to indicate the contribution of each feature in the sample (Lundberg and Lee, 2017). SHAP, a

462 game theory-based post-hoc interpretation method, quantifies the marginal impact of each feature on

463 model predictions. The SHAP summary plot in **Figure 8** (a) ranks features based on their absolute SHAP

464 values, consistent with the CatBoost importance ranking. Each row represents a feature, where red

465 indicates higher feature values and blue indicates lower values. The results show that DEM, SLOPE, and

466 NDVI negatively impact flood risk, meaning that higher elevation, steeper slopes, and greater vegetation

467 coverage reduce flood hazards. In contrast, DD, DURA, and PREC positively impact flood risk,

468 indicating that higher drainage density, longer durations of extreme rainfall, and increased precipitation

469 levels contribute to higher flood hazards. Among these, DEM has the highest absolute SHAP value, with

470 a strong clustering below zero, reinforcing its dominant role in flood risk determination.

471
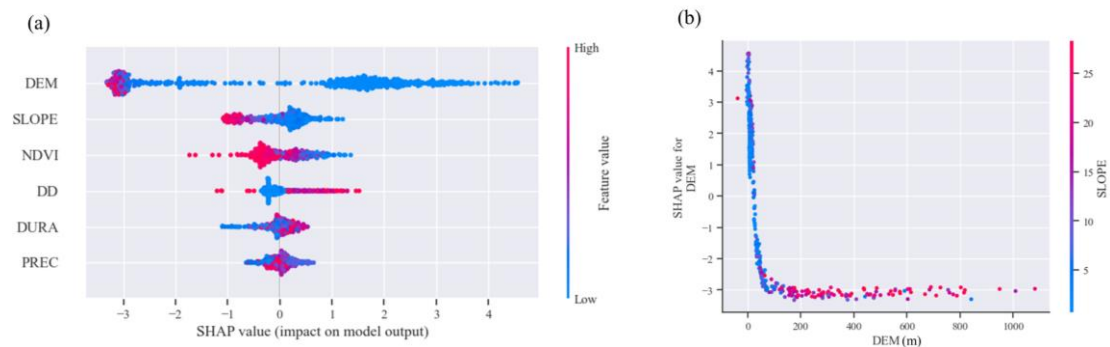
472 **Figure 8: (a) Scatter Plot of Hazard Indicators from SHAP Analysis. (b) SHAP Dual Dependence Analysis of**

473 **Elevation and Slope Factors.**

474

475 To directly capture the interaction effects between paired indicator factors, this study used SHAP

476 interaction values based on game theory, ensuring consistency while also explaining the interaction

477 effects of individual predictions. For the DEM feature, which had the highest importance in the SHAP

478 analysis, the factor most strongly correlated with it was SLOPE. Therefore, to illustrate how one feature

479 interacts with another to affect the model training results, this study used DEM and SLOPE as examples

480 to plot the SHAP interaction scatter plot, representing the dependency of the DEM feature. The results

481 are shown in **Figure 8** (b). This dependency plot takes the form of a logarithmic function, indicating that

482 as DEM increases, the flood hazard decreases. Additionally, the slope has a negative effect on the flood

483 hazard in relation to elevation; that is, at lower elevations and gentler slopes, the flood hazard is greater.

484 **3.1.3 Determination of flood risk index weights**

485 A judgment matrix was constructed for 19 indicator factors. A hazard index was constructed based on

486 feature importance calculated using AutoML. The exposure, vulnerability, and resilience indicators were

487 determined based on existing literature and relevant expert scores (Hsiao et al., 2021). Combined with

488 the actual characteristics of the YRDUA, the 1–9 scale method was used to compare item-by-item any

489 two indicators and determine their relative importances and assign weights. Finally, the judgment matrix

490 results were tested for consistency, and the CR value was 0.0058, i.e., $\ll 0.100$, indicating that the results

491 passed the consistency test and that the flood risk index weight values calculated using the AHP were

492 acceptable. The specific indicator weights and their corresponding impacts on flood risk are shown in

493 **Table 5**. The "Attribute" column represents the impact of each indicator on flood risk, with "+" indicating

494 a positive impact on flood risk and "-" indicating a negative impact on flood risk.

495 **Table 5: Flood risk index weights.**

Dimension	Indicator	Unit	Attribute	Weight
Hazard (0.4798)	PREC	mm	+	4%
	DURA	Day	+	10.8%
	NDVI		-	7.6%
	DEM	km	-	22.99%
	SLOPE	°	-	6.4%
	DD	km/km^2	+	3.2%
	AREA	km^2	+	1.1%
Exposure (0.1083)	DPOP	people/km^2	+	4.32%
	DGDP	10,000 yuan/km^2	+	3.84%
	DBUI	km^2	+	1.16%
Vulnerability (0.1312)	PPOP_CHI	%	+	4.92%
	PPOP_ELD	%	+	3.04%

Dimension	Indicator	Unit	Attribute	Weight
	PPOP_UEDU	%	+	2.11%
	UR	%	-	2.05%
	GDP per capita	100 million yuan/10,000 People	-	4.43%
Resilience (0.2807)	UEMP	%	+	5.04%
	DOCS	Per person	-	4.13%
	INSTS	Each	-	0.45%
	BEDS	Per bed	-	6.28%

496

497 The weighted results reflect the degrees of influence of the different indicator factors on flood risk.

498 Danger was the decisive factor affecting flood risk, with a weight of 0.4798, followed by resilience and

499 vulnerability. Exposure had a relatively low impact on flood risk. In terms of danger, the topography and

500 DURA were the main factors affecting the occurrence of flooding. These two indicators determined the

501 characteristics of flood disasters in the YRDUA from the perspective of disaster-prone environments and

502 driving factors, respectively. In terms of exposure, the YRDUA is a typical area with rapid social,

503 economic, and population growths in China. High population and GDP densities increase the risk of

504 flood exposure. In addition, the uneven age distribution and education levels of the population are

505 important social factors affecting the risk of flood disasters in urban agglomerations. In terms of

506 resilience, improving health and medical infrastructure, developing the regional economy, and reducing

507 unemployment rates are conducive to improving the overall disaster response capacity of the region and

508 reducing the risk of flood disasters in the YRDUA.

509 **3.1.4 Model results verification**

510 Based on CatBoost under the AutoML framework and AHP, the levels of flood hazard, exposure,

511 vulnerability, and resilience were calculated for floods in the YRDUA and the spatial distribution of

512 flood risks in the region was obtained according to the weights determined by the model. Combined with

513 the natural breakpoint classification method, a flood risk zoning map of the YRDUA was constructed.

514 The extracted flood points were superimposed on the map to verify whether the model exhibited good

flood risk assessment capabilities. The results are shown in **Figure 9**, indicating that the distribution of

flood points was consistent with the distribution of high and medium-to-high risk areas in the region,

with the model assessment results corresponding well with the actual flooding situation. To specifically

illustrate the correspondence of the results, the proportion of flood points distributed in high and medium-

to-high risk areas was quantitatively calculated. The obtained value was 87.45%, indicating that the flood

risk assessment results of the model in this study were highly credible, and subsequent analysis could be

conducted.

As shown in **Figure 9**, the high and medium-to-high risk areas in the YRDUA were mainly located in the

northern part of the region, concentrated in Chizhou, Anqing, Ma'anshan, and Xuancheng Cities in Anhui

Province, Yancheng and Yangzhou Cities in Jiangsu Province, and Taizhou City in Zhejiang Province.

Meanwhile, most areas of Hangzhou City had the lowest risk. The flood risks in cities such as Shanghai,

Nanjing, and Jinhua were also relatively low. The overall analysis showed that the flood risk in the study

area was low in the southwest and high in the northeast, determined largely by natural terrain and

meteorological factors. The spatial distribution of the flood hazard class was similar to the distribution

of flood risks; exposure decreased stepwise from Shanghai to the surrounding areas, reflecting that

densely populated and economically developed cities have higher exposure. Areas with higher

vulnerability were mainly concentrated in Chizhou, Anqing, Xuancheng, Chuzhou, and Yancheng Cities.

The number of vulnerable people in these cities was relatively high. Vulnerability has aggravated the

flood risks in Chizhou and Anqing Cities on the basis of flood risk. Meanwhile, Shanghai had the best

resilience performance, followed by those of Hangzhou, Suzhou, and Nanjing Cities, greatly lessening

the flood risks in these cities.

536
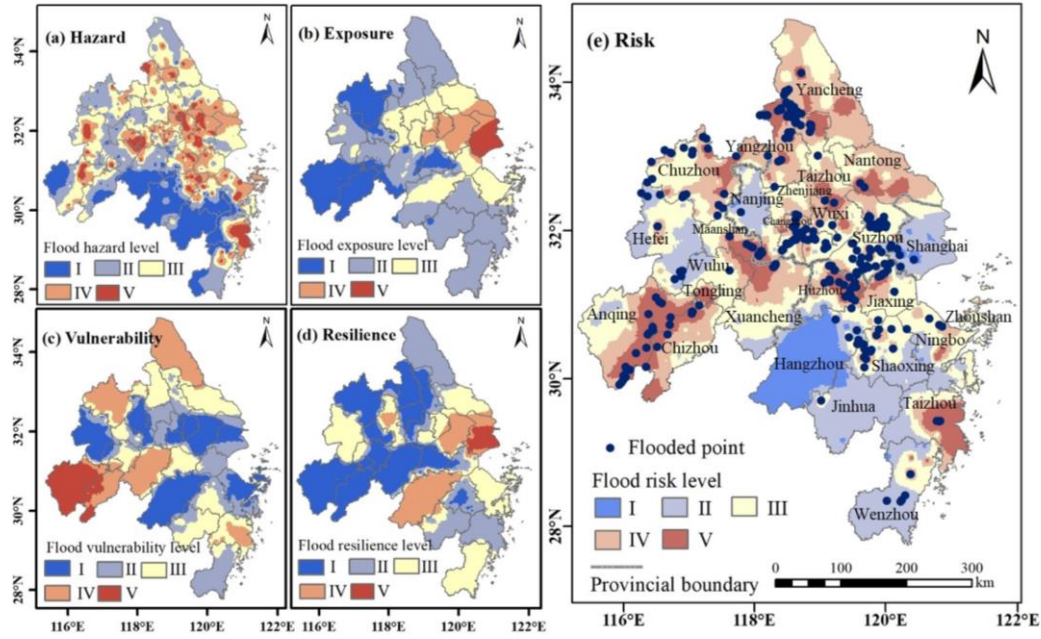
Figure 9: Flood risk level distribution and verification results based on a flood risk assessment model. The flood hazard, exposure, vulnerability, and resilience of the YRDUA were calculated using CatBoost under the AutoML framework and AHP. The flood hazard level (a), flood exposure level (b), flood vulnerability level (c), flood resilience level (d), and flood risk spatial distribution (e) were derived through natural breaks classification in ArcGIS software based on model-determined weights, resulting in a flood risk zoning map for the YRDUA.

3.2 Analysis of changes in the spatiotemporal characteristics of flood risk

The flood risk results for the YRDUA from 1990 to 2020 were obtained based on the flood risk assessment model proposed in this study. The differences in flood risk among cities in the YRDUA over the past few decades are primarily due to a complex interplay of various factors, including geographic and climatic conditions, urbanization processes, socio-economic factors, ecological changes, and historical flood events. The topography and precipitation patterns of different cities affect their capacity for rainwater drainage and accumulation, while urbanization leads to an increase in impervious surfaces and variations in infrastructure development, impacting flood management capabilities. Additionally, differences in DPOP, economic development levels, and flood management policies can exacerbate flood risk. Furthermore, the increasing frequency of extreme weather events due to climate change further elevates flood risk. These factors determine the varying levels of flood risk among cities within the YRDUA.

As the interannual difference in flood risk in the region was small and the change response was weak, we selected the flood risk results for 1990, 2000, 2010, and 2020 to analyze the changes in the spatiotemporal pattern. In this analysis, variables such as PREC and DURA exhibit clear temporal variability, as they change year by year due to weather patterns. However, other factors like DEM, SLOPE, NDVI, and urbanization indicators such as DPOP and GDP are spatial variables that do not exhibit direct temporal changes, but their effects on flood risk are influenced by changing socio-economic and ecological conditions.

Regarding spatial patterns (**Figure 10**), the flood risk in the YRDUA showed clear spatial heterogeneity. The southwestern part of the study area and Shanghai have shown low flood risks over the past 30 years, whereas the central and northern parts of the region have been more likely to face flood risks depending on the natural conditions, population, economic conditions, and recovery capacity of the region. Regarding temporal patterns, from 1990 to 2010, areas with high and medium-to-high risk decreased markedly. By 2010, most of the YRDUA (except for a few areas) was in a state of medium risk or below, with the southwestern region exhibiting a large range of low risk levels. The corresponding areas for each risk level are shown in **Figure 11**. From 1990 to 2010, areas of low and low-to-medium risk levels gradually increased, maximizing in 2010, whereas areas of medium risk and above continued to decrease. By 2020, the number of high-risk areas for flooding increased. There is a tendency for areas of medium-to-high risk in the central region to shift towards high-risk areas in 2020, as compared to the state in 1990. Meanwhile, high-risk areas for floods also appeared in Chizhou and Anqing Cities in Anhui Province, which was mainly due to the intensification of extreme weather, unbalanced population distribution, and rapid economic development in recent years.

577
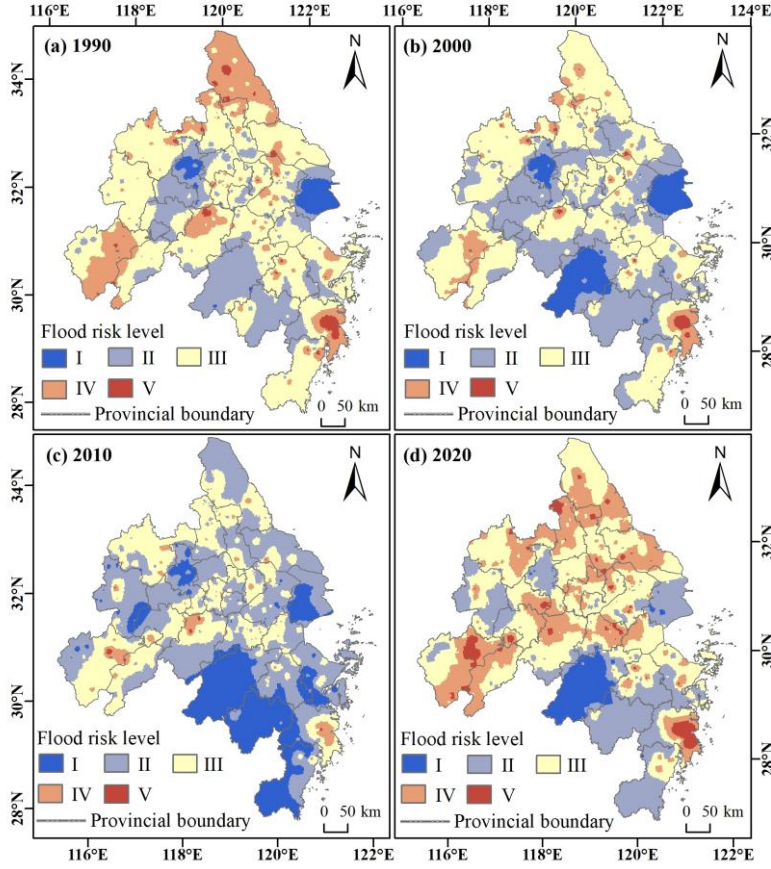
578   **Figure 10: Spatial distributions of flood risk in the YRDUA in different years during 1990–2020.**

579

580
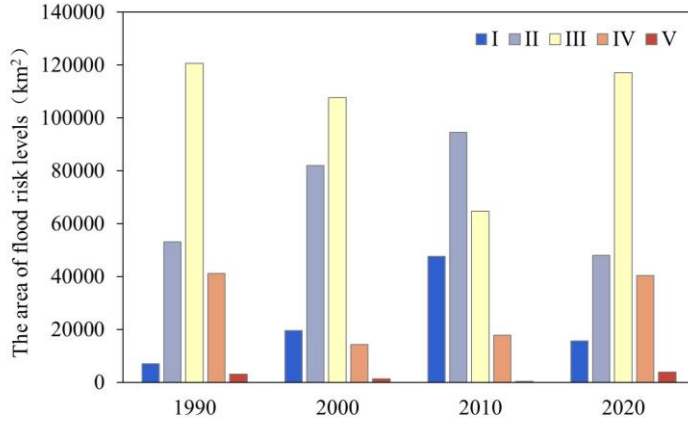
581   **Figure 11: Areas at different levels of flood risk in the YRDUA in different years during 1990–2020.**

582

583   To further analyze the changes in flood risk in the region, we calculated the change rate of the area of

584   different risk levels every 10 years and the overall change rate over 30 years. The interannual rate of

585   change was expressed in Eq. (13).

586    $R_{l,ij} = \frac{Risk_{l,j} - Risk_{l,i}}{Risk_{l,i}} \times 100\%,$ (13)

where $R_{l,ij}$ is the rate of change of the flood risk area of a certain level l in a certain year, i and j are

different years, and $Risk_{l,j}$ and $Risk_{l,j}$ are the areas corresponding to the flood risk of this level in

different years.

The interannual variation rate of the flood risk is shown in **Table 6**. Results showed that the interannual

variation between the areas of low and high risk was relatively large. The low-risk area maximized in

2010, and both R $_{2000–1990}$ and R $_{2010–2000}$ showed a positive variation rate. The high-risk area showed the

largest interannual variation rate from 2010 to 2020, reaching 12.22% and causing the high-risk flood

area in 2020 to spread, resulting in a large high-risk area.

Table 6: Interannual change rates of flood risk areas of different levels (expressed as percentages).

	$R_{2000\text{-}1990}$	$R_{2010\text{-}2000}$	$R_{2020\text{-}2010}$	$R_{2020\text{-}1990}$
I	1.77%	1.44%	-0.67%	1.21%
II	0.54%	0.15%	-0.49%	-0.10%
III	-0.11%	-0.40%	0.81%	-0.03%
IV	-0.65%	0.25%	1.25%	-0.02%
V	-0.53%	-0.80%	12.22%	0.27%

Analyzing the flood risk of the entire urban agglomeration does not reveal the spatial scale effect of flood

risk, nor does it consider the correlation and impact of flood risk at different spatial scales. To reflect the

distribution of and changes in flood risk at different spatial scales within the region, the risk intensity of

different provinces was further analyzed, and the results are shown in **Figure 12**, respectively. In **Figure

12**, the average flood risk reflects the differences in risk development of the provincial administrative

units in Shanghai, Anhui, Zhejiang, and Jiangsu in terms of time and space. Overall, all administrative

units in the YRDUA exhibited the highest flood risk in 2020, and the overall risk trend increased. At the

provincial level, Shanghai's flood risk was consistently low, showing a trend of first decreasing from

0.152 in 1990 to 0.123 in 2000 and then gradually increasing to 0.311 in 2020. Among the other three

provinces, Jiangsu and Anhui had relatively high flood risks, reaching 0.525 and 0.516, respectively, in

2020, whereas Zhejiang had a relatively low flood risk, which remained stable between 1990 and 2010,

with no distinct changes.

609
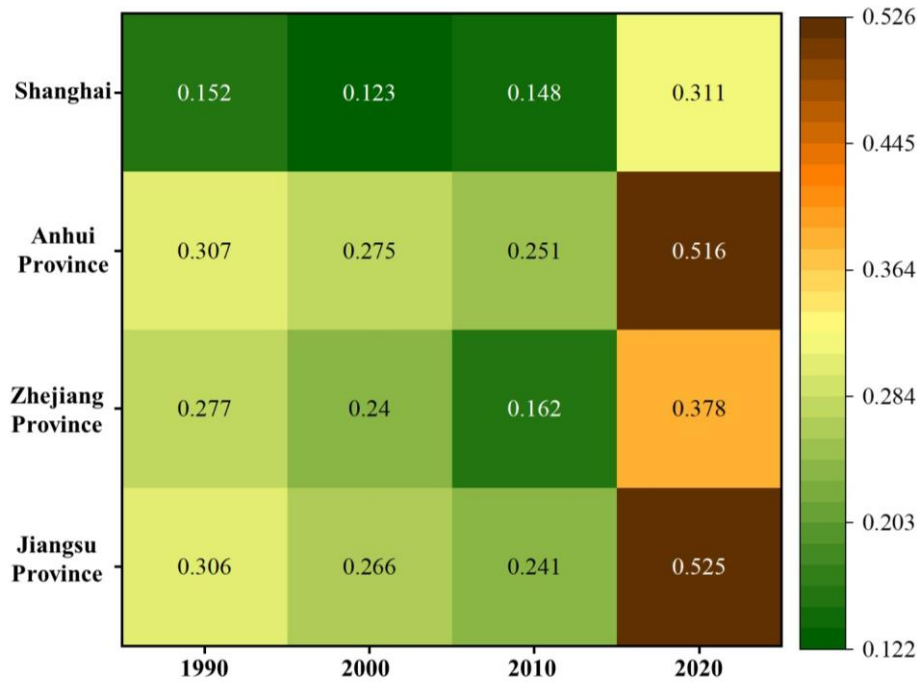
Figure 12: Distribution of Average Flood Risk in Each Province of the Yangtze River Delta Urban Agglomeration from 1990 to 2020

4 Conclusion

Flood risk assessment at the scale of urban agglomeration is a hot research topic in the field of disaster prevention and mitigation. In this study, the flood risk assessment indexes for YRDUA were determined in different dimensions of danger, exposure, vulnerability and resilience, and a flood risk assessment model based on AutoML and AHP was constructed to study the changes of spatial and temporal characteristics of flood risk in the region in the last 30 years from 1990 to 2020, aiming to provide scientific basis for the prevention and resilience of the YRDUA. The main conclusions of this study are as follows:

(1) In the flood risk calculation, the CatBoost model has the highest Precision, F1-score, and Kappa, and its Precision can reach 0.9030. Further analysis of the ROC curve and the corresponding AUC value of the model shows that its AUC value is 0.91, which indicates that the CatBoost model has the best performance and prediction reliability. Therefore, the CatBoost model was selected to calculate the flood risk in the YRDUA.

626 (2) Using the flood risk assessment model based on AutoML and AHP to obtain the flood risk of the

627 YRDUA, superimposed on the flooded point data for comparative analysis, we found that the distribution

628 of flooded points in the study area is basically consistent with the distribution of high and medium-to-

629 high risk areas of flooding, and the proportion of the distribution of the quantification of its distribution

630 is 87.45%, which indicates that the model in this study has a good performance and credibility regarding

631 the assessment of flood risk.

632 (3) The spatial distribution of flood risk in the YRDUA during the 30-year study period shows obvious

633 heterogeneity, with the southwestern part of the region and Shanghai City having a low flood risk,

634 whereas the north-central part of the region faces a relatively high probability of flood risk. Between

635 1990 and 2010, there was a substantial decrease in the high and medium-to-high risk flood zones; yet by

636 2020, there was an increase in the high-risk flood zones. There is a tendency for the medium-to-high risk

637 area in the center of the region to shift to a high-risk area, whereas high-risk areas also occur in the cities

638 of Chizhou and Anqing in Anhui Province.

639 (4) All administrative units of the YRDUA exhibited the highest flood risk in 2020, with an overall trend

640 of increasing risk. At the provincial level, Jiangsu and Anhui Provinces possess relatively high flood

641 risks, whereas Zhejiang Province has a relatively low flood risk.

642 (5) The findings of this study provide valuable insights for flood risk management and policy-making.

643 The flood risk maps generated in this study can serve as a scientific basis for urban planning,

644 infrastructure development, emergency response, and disaster prevention strategies. By integrating these

645 risk assessments into decision-making processes, government agencies and urban planners can optimize

646 flood prevention measures and enhance regional resilience. Furthermore, the AutoML framework used

647 in this study can be applied to other regions for flood risk assessment and can be integrated with future

648 climate change scenarios to enable long-term forecasting and proactive disaster mitigation strategies.

649 **Data availability.**

650 Data will be made available on request.

651 **Competing interests.**

652 The authors declare that they have no competing financial interests or personal relationships that may

653 have influenced the work reported in this study.

654 **Author contributions.**

655 **Yu Gao:** Writing - original draft preparation, Validation, Software, Methodology, Conceptualization

656 **Haipeng Lu:** Writing-review & editing, Visualization, Supervision, Formal analysis. **Yaru Zhang:**

657 Methodology, Formal analysis. **Hengxu Jin:** Writing - review & editing, Methodology. **Shuai Wu:**

658 Software, Formal analysis. **Yixuan Gao:** Visualization, Software. **Shuliang Zhang:** Writing-review &

659 editing, Resources, Project administration, Funding acquisition, Conceptualization .

660 **Acknowledgements**

661 This study was supported by the National Natural Science Foundation of China (Grant Nos. 42271483

662 and 42071364) and Jiangsu Provincial Natural Resources Science and Technology Project

663 (JSZRKJ202405). We would like to thank Editage (www.editage.cn) for English language editing.

664 **References**

665 Abu-Salih, B., Wongthongtham, P., Coutinho, K., Qaddoura, R., Alshaweesh, O., and Wedyan, M.: The

666 development of a road network flood risk detection model using optimised ensemble learning, Eng. Appl.

667 Artif. Intell., 122, 106081, https://doi.org/10.1016/j.engappai.2023.106081, 2023.

668 Adnan, R. M., Yuan, X., Kisi, O., and Anam, R.: Improving Accuracy of River Flow Forecasting Using

669 LSSVR with Gravitational Search Algorithm, Advances in Meteorology, 2017, 1–23,

670 https://doi.org/10.1155/2017/2391621, 2017.

671 Anon: Identification of sensitivity indicators of urban rainstorm flood disasters: A case study in China,

672 J. Hydrol., 599, 126393, https://doi.org/10.1016/j.jhydrol.2021.126393, 2021.

673 Aven, T.: Risk assessment and risk management: Review of recent advances on their foundation,

674 European Journal of Operational Research, 253, 1–13, https://doi.org/10.1016/j.ejor.2015.12.023, 2016.

675   Bostan, P. A., Heuvelink, G. B. M., and Akyurek, S. Z.: Comparison of regression and kriging techniques

676   for mapping the average annual precipitation of Turkey, Int. J. Appl. Earth Obs. Geoinf., 19, 115–126,

677   https://doi.org/10.1016/j.jag.2012.04.010, 2012.

678   Consuegra-Ayala, J. P., Gutiérrez, Y., Almeida-Cruz, Y., and Palomar, M.: Intelligent ensembling of

679   auto-ML system outputs for solving classification problems, Inform. Sci., 609, 766–780,

680   https://doi.org/10.1016/j.ins.2022.07.061, 2022.

681   Criado, M., Martínez-Graña, A., San Román, J. S., and Santos-Francés, F.: Flood risk evaluation in urban

682   spaces: The study case of Tormes River (Salamanca, Spain), International journal of environmental

683   research and public health, 16, 5, 2019.

684   Ding, T., Chen, J., Fang, Z., and Chen, J.: Assessment of coordinative relationship between

685   comprehensive ecosystem service and urbanization: A case study of Yangtze River Delta urban

686   Agglomerations, China, Ecol. Indic., 133, 108454, https://doi.org/10.1016/j.ecolind.2021.108454, 2021.

687   Donegan, H. A., Dodd, F. J., and McMaster, T. B. M.: A New Approach to Ahp Decision-Making,

688   Journal of the Royal Statistical Society: Series D (The Statistician), 41, 295–302,

689   https://doi.org/10.2307/2348551, 1992.

690   Echendu, A. J.: The impact of flooding on Nigeria's sustainable development goals (SDGs), Ecosyst.

691   Health Sustainability, 6, 1791735, https://doi.org/10.1080/20964129.2020.1791735, 2020.

692   Fernández, D. S. and Lutz, M. A.: Urban flood hazard zoning in Tucumán Province, Argentina, using

693   GIS and multicriteria decision analysis, Eng. Geol., 111, 90–98, 2010.

694   Gain, A. K., Mojtahed, V., Biscaro, C., Balbi, S., and Giupponi, C.: An integrated approach of flood risk

695   assessment in the eastern part of Dhaka City, Nat. Hazards, 79, 1499–1530,

696   https://doi.org/10.1007/s11069-015-1911-7, 2015.

697   Gu, C., Hu, L., Zhang, X., Wang, X., and Guo, J.: Climate change and urbanization in the Yangtze River

698   Delta, Habitat Int., 35, 544–552, https://doi.org/10.1016/j.habitatint.2011.03.002, 2011.

699   Guan, X., Yu, F., Xu, H., Li, C., and Guan, Y.: Flood risk assessment of urban metro system using

700   random forest algorithm and triangular fuzzy number based analytical hierarchy process approach,

701   Sustainable Cities and Society, 109, 105546, https://doi.org/10.1016/j.scs.2024.105546, 2024.

702   Gudiyangada Nachappa, T., Tavakkoli Piralilou, S., Gholamnia, K., Ghorbanzadeh, O., Rahmati, O., and

703   Blaschke, T.: Flood susceptibility mapping with machine learning, multi-criteria decision analysis and

704   ensemble using Dempster Shafer Theory, Journal of Hydrology, 590, 125275,

705   https://doi.org/10.1016/j.jhydrol.2020.125275, 2020.

706   Guo, Y., Quan, L., Song, L., and Liang, H.: Construction of rapid early warning and comprehensive

707   analysis models for urban waterlogging based on AutoML and comparison of the other three machine

708   learning algorithms, J. Hydrology., 605, 127367, 2022a.

709   Guo, Y., Quan, L., Song, L., and Liang, H.: Construction of rapid early warning and comprehensive

710   analysis models for urban waterlogging based on AutoML and comparison of the other three machine

711   learning algorithms, J. Hydrology., 605, 127367, https://doi.org/10.1016/j.jhydrol.2021.127367, 2022b.

712   He, X., Zhao, K., and Chu, X.: AutoML: A survey of the state-of-the-art, Knowledge-Based Systems,

713   212, 106622, https://doi.org/10.1016/j.knosys.2020.106622, 2021.

714   Hsiao, S.-C., Chiang, W.-S., Jang, J.-H., Wu, H.-L., Lu, W.-S., Chen, W.-B., and Wu, Y.-T.: Flood risk

715   influenced by the compound effect of storm surge and rainfall under climate change for low-lying coastal

716   areas, Science of the total environment, 764, 144439, 2021.

717   Jordan, M. and Mitchell, T.: Machine learning: Trends, perspectives, and prospects, Science, 349, 255–

718   260, https://doi.org/10.1126/science.aaa8415, 2015.

719   Kanani-Sadat, Y., Arabsheibani, R., Karimipour, F., and Nasseri, M.: A new approach to flood

720   susceptibility assessment in data-scarce and ungauged regions based on GIS-based hybrid multi criteria

721   decision-making method, J. Hydrol., 572, 17–31, https://doi.org/10.1016/j.jhydrol.2019.02.034, 2019.

722   Kazienko, P., Lughofer, E., and Trawinski, B.: Editorial on the special issue "Hybrid and ensemble

723   techniques in soft computing: recent advances and emerging trends," Soft Comput., 19, 3353–3355,

724   https://doi.org/10.1007/s00500-015-1916-x, 2015.

725   Khadka, D., Babel, M. S., and Kamalamma, A. G.: Assessing the Impact of Climate and Land-Use

726   Changes on the Hydrologic Cycle Using the SWAT Model in the Mun River Basin in Northeast Thailand,

727   Water, 15, 3672, https://doi.org/10.3390/w15203672, 2023.

728   Khosravi, K., Shahabi, H., Pham, B. T., Adamowski, J., Shirzadi, A., Pradhan, B., Dou, J., Ly, H.-B.,

729   Gróf, G., Ho, H. L., Hong, H., Chapi, K., and Prakash, I.: A comparative assessment of flood

730   susceptibility modeling using Multi-Criteria Decision-Making Analysis and Machine Learning Methods,

731   J. Hydrol., 573, 311–323, https://doi.org/10.1016/j.jhydrol.2019.03.073, 2019.

732   Lang, M., Barriendos, M., Llasat, M. C., Francés, F., Ouarda, T., Thorndycraft, V., Enzel, Y., Bardossy,

733   A., Coeur, D., and Bobée, B.: Use of Systematic, Palaeoflood and Historical Data for the Improvement

of Flood Risk Estimation. Review of Scientific Methods, Nat. Hazards, 31, 623–643, https://doi.org/10.1023/B:NHAZ.0000024895.48463.eb, 2004.

Li, J., Cheng, K., Wang, S., Morstatter, F., Trevino, R. P., Tang, J., and Liu, H.: Feature Selection: A Data Perspective, ACM Comput. Surv., 50, 94:1-94:45, https://doi.org/10.1145/3136625, 2017.

Lin, L., Wu, Z., and Liang, Q.: Urban flood susceptibility analysis using a GIS-based multi-criteria analysis framework, Nat Hazards, 97, 455–475, https://doi.org/10.1007/s11069-019-03615-2, 2019.

Liu Jiafu and Zhang Bai: Progress of Rainstorm Flood Risk Assessment, Geographical science, 35, 346–351, https://doi.org/10.13249/j.cnki.sgs.2015.03.013, 2015.

Lu, H., Lu, X., Jiao, L., and Zhang, Y.: Evaluating urban agglomeration resilience to disaster in the Yangtze Delta city group in China, Sustainable Cities and Society, 76, 103464, 2022.

Lundberg, S. M. and Lee, S.-I.: A Unified Approach to Interpreting Model Predictions, in: Advances in Neural Information Processing Systems, 2017.

Ma, C., Chen, Z., Zhao, K., Xu, H., and Qi, W.: Improved urban flood risk assessment based on spontaneous-triggered risk assessment conceptual model considering road environment, Journal of Hydrology, 608, 127693, https://doi.org/10.1016/j.jhydrol.2022.127693, 2022.

Mahmoud, S. H. and Gan, T. Y.: Urbanization and climate change implications in flood risk management: Developing an efficient decision support system for flood susceptibility mapping, Science of The Total Environment, 636, 152–167, https://doi.org/10.1016/j.scitotenv.2018.04.282, 2018.

Mia, Md. U., Rahman, M., Elbeltagi, A., Abdullah-Al-Mahbub, Md., Sharma, G., Islam, H. M. T., Pal, S. C., Costache, R., Islam, A. R. Md. T., Islam, M. M., Chen, N., Alam, E., and Washakh, R. M. A.: Sustainable flood risk assessment using deep learning-based algorithms with a blockchain technology, Geocarto International, 38, 1–29, https://doi.org/10.1080/10106049.2022.2112982, 2023.

Milanesi, L., Pilotti, M., and Ranzi, R.: A conceptual model of people's vulnerability to floods, Water Resources Res., 51, 182–197, https://doi.org/10.1002/2014WR016172, 2015.

Mirzaei, S., Vafakhah, M., Pradhan, B., and Alavi, S. J.: Flood susceptibility assessment using extreme gradient boosting (EGB), Iran, Earth Sci. Inf., 14, 51–67, https://doi.org/10.1007/s12145-020-00530-0, 2021.

Mishra, K. and Sinha, R.: Flood risk assessment in the Kosi megafan using multi-criteria decision analysis: A hydro-geomorphic approach, Geomorphology, 350, 106861, https://doi.org/10.1016/j.geomorph.2019.106861, 2020.

764 Morales-Torres, A., Escuder-Bueno, I., Andrés-Doménech, I., and Perales-Momparler, S.: Decision

765 Support Tool for energy-efficient, sustainable and integrated urban stormwater management,

766 Environmental Modelling & Software, 84, 518–528, https://doi.org/10.1016/j.envsoft.2016.07.019,

767 2016.

768 Munim, Z. H., Sørli, M. A., Kim, H., and Alon, I.: Predicting maritime accident risk using Automated

769 Machine Learning, Reliab. Eng. Syst. Saf., 248, 110148, https://doi.org/10.1016/j.ress.2024.110148,

770 2024.

771 Nagarajah, T. and Poravi, G.: A Review on Automated Machine Learning (AutoML) Systems, in: 2019

772 IEEE 5th International Conference for Convergence in Technology (I2CT), 2019 IEEE 5th International

773 Conference for Convergence in Technology (I2CT), 1–6,

774 https://doi.org/10.1109/I2CT45611.2019.9033810, 2019.

775 Nayak, P. C., Sudheer, K. P., Rangan, D. M., and Ramasastri, K. S.: A neuro-fuzzy computing technique

776 for modeling hydrological time series, J. Hydrol., 291, 52–66, 2004.

777 Özdemir, H., Baduna Koçyiğit, M., and Akay, D.: Flood susceptibility mapping with ensemble machine

778 learning: a case of Eastern Mediterranean basin, Türkiye, Stoch. Env. Res. Risk A., 37, 4273–4290,

779 https://doi.org/10.1007/s00477-023-02507-z, 2023.

780 Pham, B. T., Luu, C., Dao, D. V., Phong, T. V., Nguyen, H. D., Le, H. V., von Meding, J., and Prakash,

781 I.: Flood risk assessment using deep learning integrated with multi-criteria decision analysis, Knowledge-

782 Based Systems, 219, 106899, https://doi.org/10.1016/j.knosys.2021.106899, 2021.

783 Raschka, S.: Model Evaluation, Model Selection, and Algorithm Selection in Machine Learning,

784 https://doi.org/10.48550/arXiv.1811.12808, 10 November 2020.

785 Rashidi Shikhteymour, S., Borji, M., Bagheri-Gavkosh, M., Azimi, E., and Collins, T. W.: A novel

786 approach for assessing flood risk with machine learning and multi-criteria decision-making methods,

787 Appl. Geogr., 158, 103035, https://doi.org/10.1016/j.apgeog.2023.103035, 2023.

788 Saaty, T. L.: The Analytic Hierarchy Process: Decision Making in Complex Environments, in:

789 Quantitative Assessment in Arms Control: Mathematical Modeling and Simulation in the Analysis of

790 Arms Control Problems, edited by: Avenhaus, R. and Huber, R. K., Springer US, Boston, MA, 285–308,

791 https://doi.org/10.1007/978-1-4613-2805-6_12, 1984.

Sarro, F., Moussa, R., Petrozziello, A., and Harman, M.: Learning From Mistakes: Machine Learning Enhanced Human Expert Effort Estimates, IEEE Trans. Softw. Eng., 48, 1868–1882, https://doi.org/10.1109/TSE.2020.3040793, 2022.

Scott, D., Hall, C. M., Rushton, B., and Gössling, S.: A review of the IPCC Sixth Assessment and implications for tourism development and sectoral climate action, J. Sustain. Tour., 0, 1–18, https://doi.org/10.1080/09669582.2023.2195597, 2023.

Seemuangngam, A. and Lin, H.-L.: The impact of urbanization on urban flood risk of Nakhon Ratchasima, Thailand, Appl. Geogr., 162, 103152, https://doi.org/10.1016/j.apgeog.2023.103152, 2024.

Shafizadeh-Moghadam, H., Valavi, R., Shahabi, H., Chapi, K., and Shirzadi, A.: Novel forecasting approaches using combination of machine learning and statistical models for flood susceptibility mapping, Journal of environmental management, 217, 1–11, 2018.

Sinha, R., Bapalu, G. V., Singh, L. K., and Rath, B.: Flood risk analysis in the Kosi river basin, north Bihar using multi-parametric approach of Analytical Hierarchy Process (AHP), J. Indian Soc. Remote Sens., 36, 335–349, https://doi.org/10.1007/s12524-008-0034-y, 2008.

Sun, B., Fang, C., Liao, X., Guo, X., and Liu, Z.: The relationship between urbanization and air pollution affected by intercity factor mobility: A case of the Yangtze River Delta region, Environ. Impact Assess. Rev., 100, 107092, https://doi.org/10.1016/j.eiar.2023.107092, 2023.

Tang, Z., Wang, P., Li, Y., Sheng, Y., Wang, B., Popovych, N., and Hu, T.: Contributions of climate change and urbanization to urban flood hazard changes in China's 293 major cities since 1980, J. Environ. Manage., 353, 120113, https://doi.org/10.1016/j.jenvman.2024.120113, 2024.

Vincent, A. M., K.s.s., P., and Jidesh, P.: Flood susceptibility mapping using AutoML and a deep learning framework with evolutionary algorithms for hyperparameter optimization, Appl. Soft Comput., 148, 110846, https://doi.org/10.1016/j.asoc.2023.110846, 2023.

Wagenaar, D., Curran, A., Balbi, M., Bhardwaj, A., Soden, R., Hartato, E., Mestav Sarica, G., Ruangpan, L., Molinario, G., and Lallemant, D.: Invited perspectives: How machine learning will change flood risk and impact assessment, Nat. Hazard. Earth Sys., 20, 1149–1161, https://doi.org/10.5194/nhess-20-1149-2020, 2020.

Wan, H., Zhong, Z., Yang, X., and Li, X.: Impact of city belt in Yangtze River Delta in China on a precipitation process in summer: A case study, Atmos. Res., 125–126, 63–75, https://doi.org/10.1016/j.atmosres.2013.02.004, 2013.

Wang, M., Fu, X., Zhang, D., Chen, F., Liu, M., Zhou, S., Su, J., and Tan, S. K.: Assessing urban flooding risk in response to climate change and urbanization based on shared socio-economic pathways, Science of The Total Environment, 880, 163470, https://doi.org/10.1016/j.scitotenv.2023.163470, 2023a.

Wang, P., Li, Y., Yu, P., and Zhang, Y.: The analysis of urban flood risk propagation based on the modified susceptible infected recovered model, J. Hydrol., 603, 127121, https://doi.org/10.1016/j.jhydrol.2021.127121, 2021.

Wang, T., Wang, H., Wang, Z., and Huang, J.: Dynamic risk assessment of urban flood disasters based on functional area division—A case study in Shenzhen, China, J. Environ. Manage., 345, 118787, https://doi.org/10.1016/j.jenvman.2023.118787, 2023b.

Wang, Y., Liu, G., Guo, E., and Yun, X.: Quantitative Agricultural Flood Risk Assessment Using Vulnerability Surface and Copula Functions, Water, 10, 1229, https://doi.org/10.3390/w10091229, 2018.

Xu, H., Hou, X., Pan, S., Bray, M., and Wang, C.: Socioeconomic impacts from coastal flooding in the 21st century China's coastal zone: A coupling analysis between coastal flood risk and socioeconomic development, Sci. Total Environ., 917, 170187, 2024.

Yan, M., Yang, J., Ni, X., Liu, K., Wang, Y., and Xu, F.: Urban waterlogging susceptibility assessment based on hybrid ensemble machine learning models: A case study in the metropolitan area in Beijing, China, J. Hydrol., 630, 130695, 2024.

Yang, W., Xu, K., Lian, J., Ma, C., and Bin, L.: Integrated flood vulnerability assessment approach based on TOPSIS and Shannon entropy methods, Ecol. Indic., 89, 269–280, https://doi.org/10.1016/j.ecolind.2018.02.015, 2018.

Yang, X., Li, H., Zhang, J., Niu, S., and Miao, M.: Urban economic resilience within the Yangtze River Delta urban agglomeration: Exploring spatially correlated network and spatial heterogeneity, Sustainable Cities and Society, 103, 105270, https://doi.org/10.1016/j.scs.2024.105270, 2024.

Yuan, X., Chen, C., Lei, X., Yuan, Y., and Muhammad Adnan, R.: Monthly runoff forecasting based on LSTM–ALO model, Stoch. Env. Res. Risk A., 32, 2199–2212, https://doi.org/10.1007/s00477-018-1560-y, 2018.